Strong optical forces in frequency-modulated light

M. Cashen,[1] O. Rivoire,[1,*] V. Romanenko,[2] L. Yatsenko,[2] and H. Metcalf[1]
[1]*Physics and Astronomy, State University of New York, Stony Brook, New York 11794-3800*
[2]*Institute of Physics, Academy of Sciences, Prospekt Nauky 46, Kiev, Ukraine*
(Received 29 June 2001; published 16 November 2001)

Multifrequency light can be exploited to produce different forms of optical forces on atoms. Here, we demonstrate that weakly modulated light can produce forces stronger than the radiative force limit $\hbar k\gamma/2$ that can be used either for cooling or for deflection. We present various models of these forces and compare them with our measurements.

DOI: 10.1103/PhysRevA.64.063411 PACS number(s): 32.80.Pj, 42.50.Vk

I. INTRODUCTION

For the past 20 years, optical manipulation of neutral atoms has been mostly done in a single frequency laser field, often composed of several beams with different polarizations and $\vec{k}$ vectors. There are two kinds of forces, distinguished by the mechanism for excited atoms to return to their ground states. Spontaneous decay results in the dissipative radiative force whose magnitude saturates at $F_{rad}=\hbar k\gamma/2$, where $\tau \equiv 1/\gamma$ is the excited-state lifetime. Stimulated emission results in the conservative dipole force that does not saturate. It can be viewed as coming from strong gradients of the light shift or from stimulated exchange of momentum between fields of different $\vec{k}$ vectors.

Laser cooling requires both the dissipative interaction associated with spontaneous emission, and energy loss caused by an emission frequency that is higher than the absorption frequency. For a single optical frequency on a two-level atom, such as that used in atomic beam slowing or optical molasses, this energy loss is accomplished through the Doppler shift. By contrast, in a multilevel atom, optical pumping between ground states of different energies can result in fluorescence of higher-frequency light. One well-known example is polarization gradient or Sisyphus cooling [1], but even in this case, the velocity dependent part of the force is $<F_{rad}$.

We have been exploring light forces with multiple optical frequencies that not only cool, but also can be used to slow or deflect atoms [2–4]. With polychromatic light it is possible to exploit the unsaturable dipole force at one frequency for the energy loss, while spontaneous emission induced by another frequency enables the dissipation.

Exploitation of the dipole force is complicated by the fact that it reverses sign on the wavelength scale and so its spatial average vanishes, except when it is modified by ever-present spontaneous emission (such as in Sisyphus cooling). The desire to extend the spatial range of the dipole force has produced two independent proposals that used two frequencies to provide spatial rectification [5,6]. The idea was to use the light at one of the frequencies to exert a dipole optical force on the atoms. Then the light shift from the other one with very different parameters was used to spatially modulate the atomic transition frequency ω_a. This modulation reverses the sign of the light shift caused by the beam at the first frequency with approximately the same spatial period as the force, and therefore the force is rectified.

With beams of two frequencies, one of them can be intense enough to provide a strong dipole force even with large detuning so that spontaneous emission is minimized, while the other can be used for either of two purposes. In the case of Refs. [5,6], it is chosen to spatially modulate the atomic resonance frequency as discussed above, but in our case, it is weak and close to resonance so that it induces spatially modulated optical pumping (see below).

During the few years following Refs. [5,6], there were several experiments that demonstrated the spatial rectification proposed therein [7–10]. The utility of such spatial rectification is limited, however, because the laser detunings must be carefully chosen. Therefore, the Doppler shift of moving atoms limits the velocity range over which this rectification can occur.

As part of our ongoing exploration of optical forces in nonmonochromatic light [2–4], we have exploited these extra degrees of freedom to make forces substantially $>F_{rad}$ and cover a wider velocity range than the rectified force or Sisyphus cooling. Unlike Ref. [8], we choose the laser parameters so that the population difference between the ground and excited states determines the force, and we have labeled it the "population force," F_{pop}. It is not limited to the strength of F_{rad} and its velocity range and damping capability exceeds that of both the rectified and the polarization gradient Sisyphus forces. We use a strong light beam tuned well away from resonance, with weak frequency modulation chosen to put one of the sidebands close to resonance. (We ignore the other sidebands because they are weak and very far from resonance.) This modulated beam is retroreflected to form standing waves.

We therefore consider a two-level atom in two optical standing waves of different frequencies. The "carrier" frequency produces a strong light shift and dipole force from the resultant potential hills, while the weak "sideband" causes optical pumping between the dressed states of a two-level atom that have opposite light shifts. The relative spatial phase of the two standing waves is chosen so that atoms climb (descend) potential hills shifts more often than they

*Permanent address: École Normale Supérieure, 45 rue d'Ulm, 75230 Paris cedex 5, France.

descend (climb). The phase can be chosen so the force is unidirectional (deflection and slowing) or reverses with velocity (strong Sisyphus cooling).

The population force differs from Refs. [5–10] in that the light at the sideband frequency, shifted by ω_m from the carrier's frequency ω_c, is used to excite the atoms and not to rectify the dipole force by reversing the detuning. Here, the light shift caused by this sideband frequency is much smaller than the detuning of the carrier from atomic resonance $\delta_c \equiv \omega_c - \omega_a$. Since the intensity of the sideband is quite low, only one powerful laser beam is needed. Furthermore, F_{pop} is dissipative so it can be used for cooling.

This force is also different from that of Ref. [11] because it is applicable to a two-level system where polarization plays no role, the force is $\gg F_{rad}$, and we measure it directly instead of through cooling efficiency. Our method is closely related to the two-level atom cooling mechanism in intense light of Ref. [12], but here we control the position of the maximum optical pumping rate by our choice of relative phase of the sideband's standing wave, instead of being dictated by the antinodes of the single frequency light field.

In this paper, we first present an intuitive model of the origin of this large force and make qualitative comparisons with our measurements. Then we present a more formal description of atoms moving in a frequency-modulated field. Next, we present a discussion based on an approximation to the doubly dressed states of atoms in the bichromatic field. Although this approximate model is based on the stationary solutions of the atom+laser Hamiltonian, comparison of numerical calculations based on it with our measurements shows quite excellent quantitative agreement. Finally, we discuss our experiments and present the results in the light of these models.

II. MODELS

A. Intuitive model

The spatial dependence of the light shift of a two-level atom in a single optical standing wave of detuning δ and Rabi Frequency Ω is

$$\omega_{ls}(z) = [\pm\sqrt{[2\Omega(z)]^2+\delta^2} - \delta]/2, \tag{1}$$

and is not sinusoidal, even though the intensity distribution is [13]. (The factor of 2 in $2\Omega(z)$ arises because there are two traveling waves that make up the standing wave.) Typical parameters for our experiment are given in Table I, although the values of δ and Ω for the sideband can vary considerably from these.

What is important is that the low intensity of the sideband makes both its light shift and its concomitant dipole force much smaller than those of the carrier, and for this intuitive model, we neglect both of these [14]. By contrast, the sideband's excitation rate

$$\gamma_p = \frac{s\gamma/2}{1+s+(2\delta/\gamma)^2} \tag{2}$$

TABLE I. Typical values of the laser parameters for our experiments. The value of Ω^0 is the Rabi frequency for each traveling-wave component of the standing wave, whereas s_{max} is evaluated at each antinode of the standing wave field and is given by $2(2\Omega^0)^2/\gamma^2$. We calculate γ_p for the sideband at point C of Fig. 1(a) where it is exactly resonant.

Laser field	δ/γ	Ω^0/γ	s_{max}	γ_p/γ (max)	ω_{ls}/γ
Carrier	± 36.2	21	3500	0.2	10
Sideband	± 2.5	2.6	54	0.5	1.6

has a maximum where ω_a is shifted into resonance with it by the carrier. The resulting γ_p for the sideband is about 2.5 times larger than for the carrier at its antinode, as shown in Table I. We therefore neglect the effects of both excitation by the carrier and light shifts of the sidebands. [Here, the saturation parameter $s \equiv I/I_{sat} = 2\Omega^2/\gamma^2$ and $I_{sat} \equiv \pi hc/3\lambda^3\tau \sim 160\ \mu\mathrm{W/cm^2}$ for our $2\,^3S_1 \rightarrow 2\,^3P_2$ transition in metastable He (He*) at $\lambda = 1083$ nm.]

To understand how the population force arises, we first consider the relative spatial phase of the standing waves as shown in Fig. 1(a). Excitation occurs primarily along the path represented by the line CD so atoms experience a maximum force $F_{max} = \Delta E/\Delta z = f\hbar\omega_{ls}/(\lambda/2\pi) \sim 15F_{rad}$. Since the line CD is not located at a node, and since atoms do not necessarily decay at an antinode, the fraction f is estimated to be about $f \sim 3/4$ [see Fig. 1(a)] [15]. [Excitation along AB is

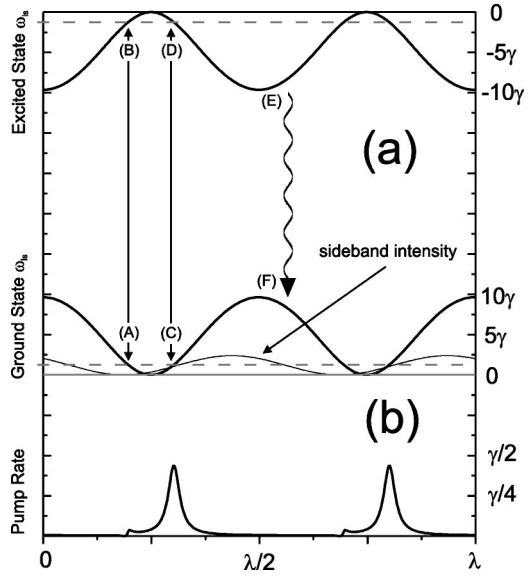

FIG. 1. Part (a) shows the light shifts for the ground and excited states (solid lines), and the detuning of the sideband (horizontal dashed line). The vertical arrows AB and CD show the places where the sideband light is resonant with the atomic transition. The small-amplitude sine wave plotted with the ground state shows the sideband's spatial intensity distribution. Part (b) shows the excitation rate $\gamma_p^s(z)$ for the sideband. It is extremely tiny near point (A) because of its node, but nearly saturates near point (C). For these plots, the laser parameters are those given in Table I, with $\delta_c > 0$, $\delta_s < 0$, and $\chi = \pi/4$.

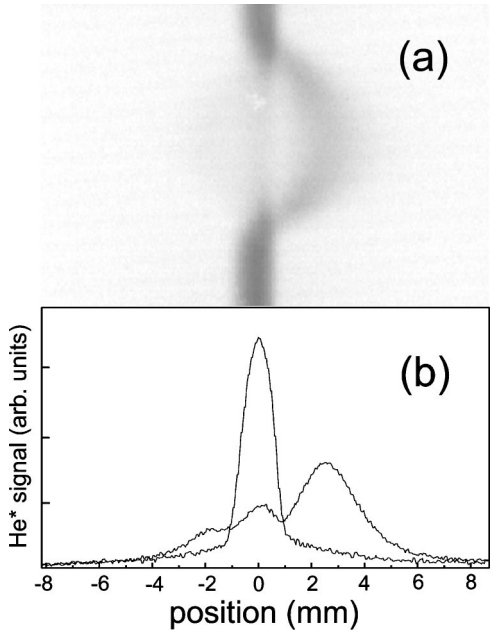

FIG. 2. The upper part is a single-frame image (no averaging) of the phosphor screen illuminated by electrons amplified by the MCP that are emitted by impact of He* atoms (with laser light on). The laser parameters are the same as for Fig. 1 (Table I) and the interaction time was 35 τ. Atoms hitting near the top and bottom of the screen do not pass through the laser beam and therefore serve as markers for undeflected atoms. The prominent bulge to the right shows the strongly deflected atoms, and there is a (hard-to-see) much weaker bulge to the left that is attributed to atoms with initially high speeds to the left. Part (b) shows two intensity traces across part (a), with and without the laser beams. The lower one of these shows two groups of atoms deflected in opposite directions, and its central peak is from uv light from the discharge in the source. [The left bulge does not show well in part (a) but its trace is clear in part (b).]

strongly inhibited because A is near the node of the sideband as shown in Fig. 1(b).] If atoms moving to the right decay along a path EF, they will gain even more kinetic energy before they reach the next point equivalent to (C) just beyond $3\lambda/4$ where they can be excited again [15]. Thus, for a range of velocities of the order of γ/k, moving atoms generally experience a strong deflection force to the right. Of course, faster atoms will move further than $\lambda/2\pi$ (distance DE) before decaying to the ground state and thus will experience an average $\Delta E \sim f\hbar\omega_{ls}/2$. Since ΔE is smaller and the distance traveled is larger, such faster atoms will experience a correspondingly smaller force that decreases as $1/v$. In Fig. 2, we show a measured atomic beam deflection corresponding to a force of $\sim 2.2F_{rad} \sim F_{max}/7$, and this seems quite realistic since it is averaged over velocities of several times γ/k.

By contrast, choosing the phase so that atoms are primarily excited from the hilltops of the ground state to the valleys of the excited-state potential results in strong Sisyphus cooling. In this case, the carrier is detuned to the red so its nodes correspond to hilltops for the ground state, and it is precisely at these points where the sideband most effectively

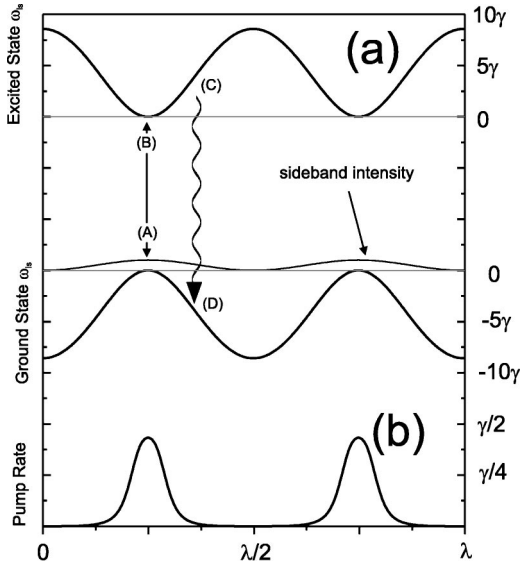

FIG. 3. Sisyphus cooling example. Part (a) shows the spatial dependence of the opposite light shifts for the ground and excited states of a two-level atom. The sideband intensity is also plotted just above the ground state to show that its spatial phase makes excitation most likely along the line AB. For atoms moving in either direction, spontaneous emission is most likely to occur from a higher energy point than (B), for example along the path CD, radiating more energy than was absorbed. Here, $\Omega_c^0 = 20\gamma$, $\Omega_s^0 = 1.4\gamma$, $\delta_c = -38\gamma$, $\delta_s = +0.6\gamma$, and $\chi = \pi$.

excites atoms, as shown in Fig. 3. Since atoms arrive in the excited state at the potential minima, they climb more hills than they descend, and there is strong Sisyphus cooling. Collimation of our atomic beam under these conditions is shown in Fig. 4.

Clearly these intuitive pictures of the origin of this strong force can provide qualitative descriptions of our measurements, and also serve as a guide to developing new ideas along similar lines.

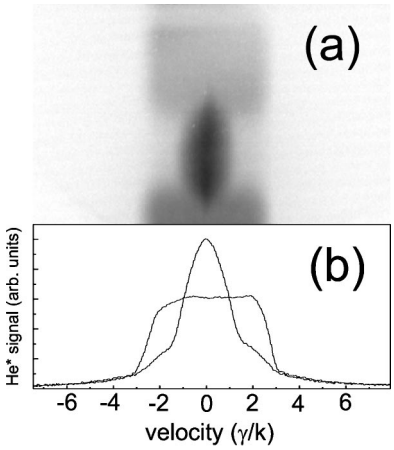

FIG. 4. Part (a) shows an image of the MCP-illuminated screen (again, single frame with no averaging), and part (b) a plot of the atomic flux across a horizontal line of part (a) (with and without the laser beams) when the parameters are chosen for Sisyphus cooling. The laser parameters are the same as those of Fig. 3, and the interaction time was $\sim 100\tau$.

B. Optical fields and forces

1. Effective Hamiltonian

We seek a solution for the force on two-level atoms moving in the field of two counterpropagating frequency-modulated laser waves. The electric field $\vec{\mathcal{E}}_i(z,t)$ of the frequency-modulated plane waves traveling in the positive $(i=1)$ and negative $(i=2)$ directions can be written as

$$\vec{\mathcal{E}}_{1,2}(z,t)=\mathcal{E}_0\hat{\varepsilon}\cos[\mp kz+\omega_c t+\beta\sin(\omega_m t\pm\chi/2)], \quad (3)$$

where $\hat{\varepsilon}$ is the unit polarization vector and $\mathcal{E}_0$ is the time-independent amplitude of the waves. The waves have an equal modulation index $\beta=\delta_0/\omega_m$, where δ_0 is the range of the frequency sweep. The only difference in modulation properties are phase differences χ of each wave. For the particular case of $\beta\ll 1$, the sum of the fields in Eq. (3) can be
considered as three standing waves: a central strong component with carrier frequency ω_c and electric field $2\mathcal{E}_0[\cos\omega_c t][\cos kz]$, and two sidebands with frequencies $\omega_c\pm\omega_m$ and electric fields $\pm\beta\mathcal{E}_0[\cos(\omega_c\pm\omega_m)t][\cos(kz\mp\chi/2)]$. The spatial phase shift of the sidebands with respect to the carrier is $\pm\chi/2$ for the low-frequency (high-frequency) sideband, respectively.

In the rotating wave approximation, the Hamiltonian $\mathcal{H}(z,t)$ describing a two-level atom interacting with the field $\vec{\mathcal{E}}_{1,2}(z,t)$ is given by

$$\mathcal{H}=\frac{\hbar}{2}\begin{bmatrix}0 & \Omega_{eff}^{*}\\ \Omega_{eff} & -2\delta_c\end{bmatrix}, \quad (4)$$

where $\delta_c=\omega_c-\omega_a$ is the detuning of the carrier frequency ω_c from the atomic frequency ω_a. The effective Rabi frequency $\Omega_{eff}(z,t)$ is given by

$$\Omega_{eff}(z,t)=\sum_n 2\Omega_R J_n(\beta)e^{-in\omega_m t}\cos(kz-n\chi/2), \quad (5)$$

where $\Omega_R\equiv-(\hat{\varepsilon}\cdot\vec{d})\,\mathcal{E}_0/\hbar$ and $\vec{d}$ is the atomic dipole moment matrix element (chosen so that Ω_R is real and positive). The quantities $\Omega_R J_n(\beta)$ are the Rabi frequencies for the running waves of the spectral components n with the frequencies $\omega+n\omega_m$ that appear in the Fourier expansion of the frequency modulated field of Eq. (3).

The force exerted on atoms can be calculated from $F=-\mathrm{tr}(\rho\nabla\mathcal{H})$ where ρ is the density matrix that satisfies the optical Bloch equations. For arbitrary velocities and Rabi frequencies, these equations can be solved only numerically, and their numerical integration requires much time for averaging of the result and for waiting for the steady-state formation. So instead of direct integration of these optical Bloch equations, we used another approach based on the Fourier expansion of the density-matrix elements over $\omega_m t$ in time and over kz in space. Therefore, we seek the steady-state solution of the density-matrix equation as

$$w(z,t)=\sum_{l,m} w^{(l,m)}e^{-i(l\omega_m t+mkz)}, \quad (6)$$

and

$$\rho_{12}(z,t)=\sum_{l,m}\rho_{12}^{(l,m)}e^{-i(l\omega_m t+mkz)}, \quad (7)$$

where $w(z,t)\equiv\rho_{22}(z,t)-\rho_{11}(z,t)$. Then there arises an infinite set of linear equations for $w^{(l,m)}$ and $\rho_{12}^{(l,m)}$, and our approach is truncation of these for some values of m and l.

We address the case of large modulation frequency ω_m where excitation of the atom is produced by only one particular component n_0 that is tuned near the atomic resonance, and all the nonresonant components are so far detuned that they can only cause light shifts. Therefore we assume that all frequencies in the problem are small compared with ω_m:

$$\Omega_R,\ kv,\ \gamma,\ |\Delta|\ll\omega_m, \quad (8)$$

where $\Delta=\delta_c+n_0\omega_m$ is the detuning of the frequency of the component n_0 from the atomic resonance.

In this case there are two different time scales for the density-matrix motion. There is a fast one at ω_m and a slower one determined by all the other small frequencies. We use a standard procedure for averaging over the fast motion [16] and obtain the slow motion of the atom as described by the effective Hamiltonian $\mathcal{H}_{eff}$ given by

$$\mathcal{H}_{eff}=\frac{\hbar}{2}\begin{bmatrix}2S & \Omega_0\\ \Omega_0 & -2(\Delta+S)\end{bmatrix}. \quad (9)$$

Here $\Omega_0(z)=2\Omega_R J_{n_0}(\beta)\cos(kz-n_0\chi/2)$ is the Rabi frequency for the sideband n_0 and

$$S=\sum_{n\neq n_0}[\Omega_R J_n(\beta)\cos(kz-n\chi/2)]^2/(n-n_0)\omega_m \quad (10)$$

is an approximate expression for the light shift produced by all other spectral components.

2. Force in the frequency modulated field

Thus the problem of a two-level atom in a polychromatic field in this approximation is reduced to the problem of the interaction of the standing wave fields of particular frequency components with atoms whose transition frequency is spatially modulated by the light shift $\hbar S$. The force $F(z)$, time averaged over the fast motions, can be represented as a sum $F(z)=F_{rect}+F_{pop}$ where

$$F_{rect}=-\hbar\,\mathrm{Re}\left(\bar{\rho}_{12}\frac{\partial\Omega_0}{\partial z}\right)\quad\text{and}\quad F_{pop}=\hbar\bar{w}\frac{\partial S}{\partial z}. \quad (11)$$

Here $\bar{\rho}_{12}$ and $\bar{w}=\bar{\rho}_{22}-\bar{\rho}_{11}$ are the density-matrix elements for atoms described by the effective Hamiltonian of Eq. (9).

For the specific case of an atom at rest $(v=0)$, these position-dependent forces can be found analytically from the steady-state solutions of the optical Bloch equations. We recover the velocity-independent Eqs. (2a) and (2b) of Ref. [8]

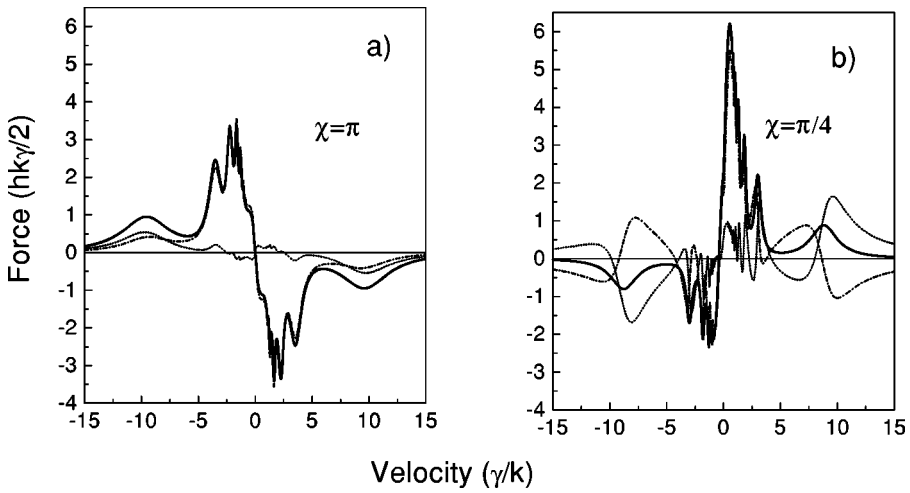

FIG. 5. Plots of the force calculated by solving the density-matrix equations for atoms described by the effective Hamiltonian Eq. (9) and using Eqs. (11). In these calculations for part (a), ($\chi=\pi$) the laser parameters are the same as those of Fig. 3 and for part (b), ($\chi=\pi/4$) they are given in Table I. In both parts, the dash-dot lines are for F_{pop}, the dotted lines are for F_{rect}, and the full lines are for total force $F=F_{pop}+F_{rect}$.

$$F_{rect}=-\hbar\frac{(\Delta+2S)}{\gamma^2+4(\Delta+2S)^2}\frac{1}{1+s}\frac{\partial\Omega_0^2}{\partial z} \tag{12}$$

and

$$F_{pop}=-\hbar\frac{1}{1+s}\frac{\partial S}{\partial z}, \tag{13}$$

where we define $s\equiv\Omega_0^2/[(\Delta+2S)^2+\gamma^2/4]$ as the saturation parameter.

The force F_{rect} is the ordinary spatially dependent dipole force. Since the detuning from the resonance is affected by the light shift $S(z)$ caused by all the other spectral components, the spatial average of $F_{rect}\neq 0$ when there is a well-chosen phase shift between $S(z)$ and $\Omega_0(z)$. This is exactly the rectification of the dipole force predicted by Kazantzev in 1987 [5].

The origin of the force F_{pop} is quite different. First, the sign of this force is different in the ground and in the excited states so the net force on the atom depends on $\bar{w}(z,t)$, which is governed primarily by the nearly resonant spectral component $\Omega_0(z)$. Second, the maximum value of these two forces is determined by different parameters. For F_{rect}, it is the amplitude of Ω_0 whereas for F_{pop} it is the amplitude of S. As with F_{rect}, the spatial average of F_{pop} does not vanish for an appropriate relative spatial phase between $S(z)$ and $\Omega_0(z)$.

If we consider the special case where the light shift induced by all the other components is small, we can expand the total force $F(z)$ over the small parameter $\Omega_R^2/\gamma\omega_m$. Only then is it possible to average the total force over z and find (not F_{pop} and F_{rect} separately)

$$F_{av}=\hbar k\frac{\Omega_R^2}{\omega_m}\times\sum_{n\neq n_0}\frac{J_n^2(\beta)\sin\chi(n-n_0)}{(n-n_0)}\frac{4s_{n_0}}{(1+\sqrt{1+4s_{n_0}})^2}$$
$$\times\left[1+\frac{\gamma^2-4\Delta^2}{(4\Delta^2+\gamma^2)\sqrt{1+4s_{n_0}}}\right], \tag{14}$$

where $s_{n_0}=[\Omega_R J_{n_0}(\beta)]^2/2[\Delta^2+\gamma^2/4]$ is the saturation parameter of each of the two beams that form the standing wave $\mathcal{E}_{n_0}$. The expression for the force exerted on moving atoms cannot be found analytically.

In general, however, the average of F_{rect} and F_{pop} over wavelength for $v\neq 0$ can only be done numerically by solving the density-matrix equations for atoms described by the effective Hamiltonian [Eq. (9)] and then using Eqs. (11). We need to use the constant velocity approximation to find the average force even though it is valid only when the atomic kinetic energy is much larger than any potential barriers (e.g., the light shift, $\hbar\omega_{ls}$). Thus, $Mv^2/2\gg\hbar\omega_{ls}$ and may be written as $kv\gg 2\sqrt{\omega_r\omega_{ls}}=\omega_{osc}$, where kv is Doppler shift and $\omega_r\equiv\hbar k^2/2M$ is the recoil frequency. This is not always a good approximation to our experimental conditions, but is adequate over a wide range of velocities and positions. This result is distinctly different from the $v=0$ case of Ref. [8].

Figure 5 shows the numerical results for two different phases. It is clear from part (a) ($\chi=\pi$) that F_{pop} dominates everywhere and furthermore is $\gg F_{rad}$. It changes sign with velocity, and thus has the properties of a very strong optical molasses. This is the Sisyphus force of Sec. II A above. Part (b) ($\chi=\pi/4$) shows that F_{pop} also dominates at low velocities, but does not change sign at $v=0$. Thus, it constitutes a strong deflection force. However, it vanishes for $v>$few times γ/k because F_{pop} and F_{rect} are of comparable magnitude but opposite sign. This may make it less useful experimentally.

C. Doubly dressed atom

In our experiment, atomic kinetic energies are often less than the height of the potential barrier produced by the light shift. Thus, the atomic velocities are strongly affected by the light shift, and it is not realistic to assert that an atom maintains a constant velocity. Therefore, we consider the evolution of atoms in the energy levels dressed by the standing waves of the carrier and sideband.

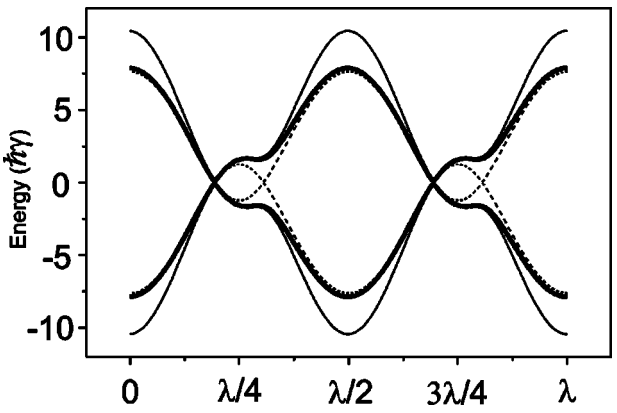

FIG. 6. This figure shows the energies of a dressed pair of levels derived from the effective Hamiltonian of Eq. (9) (thin line) and doubly dressed atom of Eq. (15) (thick line) for typical experimental parameters as given in Table I, with $\chi=\pi/4$. The dashed line represents the noninteracting energy levels which determine the slope p_i needed to calculate the Landau-Zener transition probability.

The dressed atom picture has provided an accurate description of atomic motion under the influence of the dipole force from a strong monochromatic standing wave [17]. In this model, we consider a two-level system with dressed energies E_1 and E_2 and transition rates Γ_1 and Γ_2 between these, all of which depend on the positions of atoms in the two standing waves. Atoms that interact with such a light field, experience an adiabatic force that derives from the energy shifts, $F_j=-dE_j/dz$, $j=1,2$.

One way to approximate the energies E_1 and E_2, is to use the eigenvalues of the effective Hamiltonian Eq. (9) and calculate the decay rates Γ_1 and Γ_2 following the procedure of [17]. This accounts for the strong forces that come from the light shift of the carrier's standing wave and the mixing of the ground and excited states caused by the sideband's standing wave. These energies E_1 and E_2 are plotted versus position in Fig. 6 (thin line). Use of these energies ignores mixing of ground and excited states caused by the carrier, and also depends on a formula for the light shift that is valid only for $\Omega_R \ll \omega_m$.

A different method to approximate the energies is to use doubly dressed atomic states. The energy levels of a doubly dressed atom can be obtained analytically for certain special cases by diagonalizing an infinite tridiagonal matrix [18] or using a semiclassical approach [19], but we use a different approach consisting of ''dressing the dressed states'' [20]. To do this, we first dress the atom with the light from the carrier and obtain the familiar energy levels $E_\pm$ for these two dressed states $|(+,n)\rangle$ and $|(-,n)\rangle$ using the $\pm$ terms of Eq. (1) [21]. Here, the extra set of parentheses indicates that these are the states formed by the mixing of $|g,n\rangle$ and $|e,n-1\rangle$.

The presence of a second field (sideband) with a different frequency causes many changes [22]. First, its quantum number must be part of the label of the eigenstates of the system, so $|(\pm,n)\rangle\otimes|m\rangle\equiv|(\pm,n),m\rangle\rightarrow|(j,n,m)\rangle$ where n represents the carrier and m represents the sideband ($j=1$, 2).

Now the energy levels are

$$E_{1,2}=\hbar(\delta_s\pm\sqrt{\Omega_{dd}^2+\delta_{dd}^2})/2, \tag{15}$$

where $\delta_{dd}=\delta_s-\delta_c+\Omega_c'$, $\Omega_{dd}=\Omega_s(1+\delta_c/\Omega_c')/2$, and $\Omega_c'\equiv\sqrt{\delta_c^2+\Omega_c^2}$. Here, the effective detuning for the sideband δ_{dd} includes the light shift caused by the carrier but not vice versa because the sideband's light shift is so very much smaller than δ_c [8]. Since the spatial phases of the two standing waves are not necessarily the same, we need to be careful to include their relative phase χ as

$$\Omega_c(z)=2\Omega_c^0\cos(kz) \quad \text{and} \quad \Omega_s(z)=2\Omega_s^0\cos(kz-\chi/2). \tag{16}$$

We find the rates of population transfer caused by spontaneous emission processes to be [23]

$$\Gamma_1=\gamma\left(\frac{1}{4}\sin^2 2\phi\sin^2 2\theta+\sin^4\phi\sin^4\theta+\cos^4\phi\cos^4\theta\right)$$

and

$$\Gamma_2=\gamma\left(\frac{1}{4}\sin^2 2\phi\sin^2 2\theta+\sin^4\phi\cos^4\theta+\cos^4\phi\sin^4\theta\right). \tag{17}$$

Here, the mixing angles θ and ϕ are given by [23]

$$\cos 2\theta=-\delta_c/\Omega_c' \quad \text{and} \quad \cos 2\phi=-\delta_{dd}/\Omega', \tag{18}$$

where $\Omega'=\sqrt{\delta_{dd}^2+\Omega_{dd}^2}$.

The spatial dependence of the energy levels calculated for the doubly dressed atom from Eq. (15) are shown in Fig. 6 (thick line). The effective Hamiltonian energy levels of Eq. (9) have a larger light shift at the carrier antinode (0, λ/2, and λ) than the doubly dressed states of Eq. (15) because of the approximate expression for the light shift in the effective Hamiltonian of Eq. (10), especially at the antinode where $\delta_c\sim 1.5\,\Omega_c$. The energy levels show small, unequal anticrossings that result from coupling where the carrier's light shift makes the weak sideband exactly resonant with the light-shifted atomic energy level spacing [points *A* and *C* in Fig. 1(a)]. Since the sideband's node is very close to one, but not both, of these resonance positions, the anticrossings look quite different.

When an atom moving on an energy level approaches one of these anticrossings, it can make a Landau-Zener transition to the other level. The probability of such a transition is $P(v)=\exp[-(2\pi V^2)/(\hbar v|p_1-p_2|)]$ where v is the atomic velocity, $2V$ is the energy splitting at the anticrossing and p_i is the slope of a noninteracting energy level [24] shown in Fig. 6 (shown by dashed lines).

From the point of view of the dressed atom energy levels, one can understand the asymmetry that gives rise to F_{pop} for the case $\chi=\pi/4$ in Fig. 7. Consider ground-state atoms starting at the carrier standing wave node at λ/4. If they have a small velocity v_+ to the right, adiabatic following at point

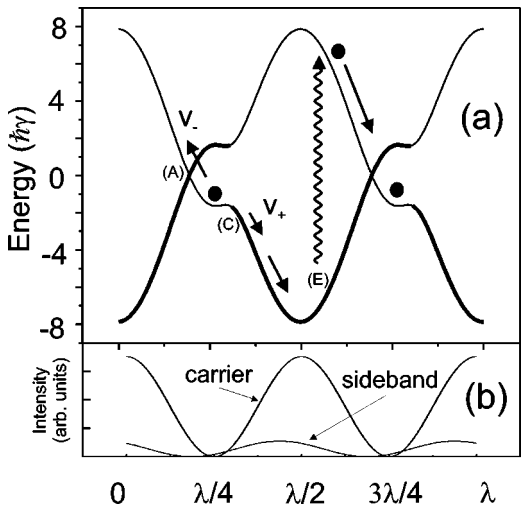

FIG. 7. In part (a), the dressed energy levels and the laser parameters are the same as those of Fig. 6, derived from the doubly dressed atom model. Here, the thicker lines indicate which doubly dressed state contains the larger fraction of the excited state (and therefore has the larger decay rate). The points (*A*) and (*C*) correspond to resonance between the light-shifted atomic transition and the sideband frequency, just as in Fig. 1. The thickness of the lines changes here because of the sign change of the detuning that switches the identity of ground and excited states in the dressed atom basis. The asymmetry that produces a unidirectional force for $\chi=\pi/4$ is clearly illustrated. Atoms traveling to the right from the carrier node at $\lambda/4$ traverse point (*C*) adiabatically to the excited state where they experience a large acceleration before decay. By contrast, atoms traveling in the opposite direction from $\lambda/4$ undergo a Landau-Zener transition and are weakly decelerated. Part (b) shows the intensity of the carrier and sideband (multiplied by ten relative to carrier here) to indicate their relative intensity.

(*C*) corresponds to excitation from the ground state. In the intuitive model described in Fig. 1, this is the point where the excitation rate is maximum along path *CD*. The atoms are accelerated to the right by the light shift potential of the excited state, and if they decay near point (*E*) (note: arrow upwards!) they will gain even more kinetic energy as they roll down the ground-state potential before they reach the next carrier node at $3\lambda/4$. By contrast, atoms moving to the left with v_- from $\lambda/4$ will make Landau-Zener transitions at point (*A*). In the intuitive model, this point corresponds to the much smaller of the two maxima in the excitation rate [path *AB* of Fig. 1(a)]. Such atoms experience a deceleration from the light shift potential. To validate this model, we performed numerical simulations that are described in Sec. III C.

III. EXPERIMENTS

We implemented these forces using amplified light from a diode-pumped fiber amplifier [25] that originates from an external cavity-stabilized SDL-6702-H1 diode laser. The diode laser frequency was locked to atomic resonance by saturated absorption spectroscopy in a static cell with a weak rf discharge. The light was weakly modulated by an EOM at $\omega_m \approx 2\pi \times 63$ MHz. The laser was typically locked ≈ 63 MHz$\approx 40\gamma$ above or below atomic resonance to place either one of the first-order sidebands close to atomic resonance.

The output beam of the EOM was injected into a diode-pumped fiber amplifier to produce several hundred mW of frequency-modulated light. The output beam of the fiber amplifier was subsequently circularly polarized to pump atoms into the $M_J=1$ sublevel of the $2\,^3S_1$ state and drive the closed transition to the $2\,^3P_2$, $M_J=2$ sublevel. The beam was apertured by an adjustable vertical slit, was incident perpendicularly onto the horizontal atomic beam, and was retroreflected by a mirror located ~ 1 m away to produce the desired relative phase of the two standing waves.

Our atomic beam source has been described in Ref. [4] but is briefly reviewed here. It is modeled after the reverse flow design of Kawanaka *et al.* [26] with modifications originated by Mastwijk *et al.* [27]. It consists of a 1 cm diam. quartz tube with a 1 mm diam. tungsten needle along its axis and a 3 cm diam. liquid-N_2-cooled stainless-steel coaxial jacket. The plasma from a dc discharge produces about $\sim 10^{14}$ He* atoms/s with a velocity distribution typical of ~ 150 K that we have characterized using a time-of-flight method with a tuning-fork beam chopper. The atoms pass through a vertical slit to define and collimate the beam and thereby enable one-dimensional (1D) transverse measurements of atomic deflection and/or laser cooling.

For these experiments, we use a multichannel plate (MCP) and phosphor screen combination to detect the He* atoms 70 cm away from the interaction region, and infer their transverse velocity distribution from their spatial distribution. Since He* atoms carry about 20 eV of internal energy, they eject an electron from the upstream surface of the MCP with high probability, and the amplified pulses at the output side of the MCP are accelerated to the screen. The screen was viewed through a window by a video camera connected to a PC via a frame grabber card. To characterize the apparatus we did several ordinary Doppler deflection experiments with a single laser beam using a wide range of laser parameters, and compared the measurements with straightforward calculations [13]. The agreement was excellent in every detail.

A. Population force

To demonstrate the population force $F_{pop} \gg F_{rad}$, we adjust the retroreflection mirror for a spatial phase of $\chi \approx \pi/4$ for the sideband as shown in Fig. 1(a). Because of the asymmetry of $\gamma_p^s(z)$ about the carrier standing wave nodes, atomic excitation is restricted to the neighborhood of position (*C*) in Fig. 1(a). Slow atoms roll down the excited-state potential from (*D*) and are accelerated to the right [15].

Thus, there is a force of magnitude $\gg F_{rad}$ exerted on the atoms over velocity range from $v \sim 0$ to $v \sim$ few times γ/k where the Doppler shift plays an important role for δ_s. Only atoms moving to the left with sufficiently high velocity will not experience this force, but instead will be accelerated to the left by a similar mechanism. In our experiments whose typical results are shown in Fig. 2, we also see such atoms that are moving in this opposite direction.

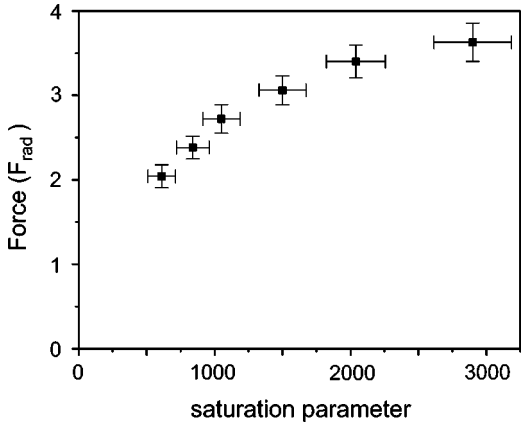

FIG. 8. The measured value of the deflection force is not only significantly larger than F_{rad}, but also does not saturate near $F=F_{rad}$. Here, $\delta_c=36.2\gamma$ and $\delta_s=-2.5\gamma$, $\beta=0.25$ so that $\Omega_s^0/\Omega_c^0=1/8$. The interaction time for these measurements was 28τ. Although the force is clearly larger than F_{rad}, it does appear to saturate at $4F_{rad}$. This is not a force saturation, however, but a result of approaching the limit of the velocity range (see text).

Figure 2(a) shows the image of the He* beam deflected by this force. Atoms at the top and bottom do not pass through the laser light and thereby provide a reference for the undeflected beam. From geometry and the mean longitudinal velocity of 1000 m/s, the 2.5 mm deflection corresponds to an imparted transverse velocity of $\Delta v\approx 3.6$ m/s$=2.0\gamma/k$, demonstrating the large velocity range. The interaction time is limited by a 3.5 mm slit aperturing the laser beam to $\approx 3.5\mu$s$\approx 35\tau\approx 0.9/\omega_r$, so $\Delta v\approx 2.0\gamma/k$ corresponds to $F\approx 2.2F_{rad}$.

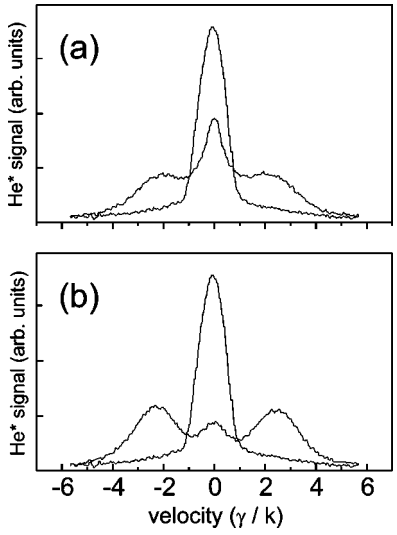

FIG. 9. Here, the laser parameters are chosen so that the Sisyphus force heats the atoms, thus showing both heating and channeling. The laser parameters for parts (a) and (b) are $\Omega_c^0=20\gamma$, $\Omega_s^0=1.2\gamma$, and phase$=\pi$. The interaction time is $\approx 100\tau$. For part (a), $\delta_c=35.6\gamma$ and $\delta_s=-3.4\gamma$ so there is not much chance for atoms to escape channeling. For part (b), $\delta_c=38\gamma$ and $\delta_s=-1\gamma$ so that there are far fewer channeled atoms. The central peak is from uv light from the discharge in the source.

In addition, Fig. 8 shows how the force increases with saturation parameter, showing no saturation at $F\sim F_{rad}$, in stark contrast with the radiative force. Its apparent saturation at $4F_{rad}$ is a result of approaching the limit of the velocity range. This is easily seen by considering from Fig. 1 that the excitation region spans only $\lambda/12$ and that the transition is strongly saturated so that $\gamma_p\approx\gamma/2$. For interaction time of 28τ, the number of excitations is $(28\tau)(\gamma/2)(\lambda/12)/(\lambda/2)\sim 2.4$. Thus, the total energy gain averages $2.4\times\omega_{ls}\sim 24\hbar\gamma$ at the maximum intensity. This corresponds to a velocity of about $3\gamma/k$, the limit shown in Fig. 5. This can be understood intuitively because a velocity of $3\gamma/k$ corresponds to traveling a distance $\lambda/2$ in a time τ, just enough to destroy the origin of the force as described by Fig. 1.

B. Sisyphus cooling

In a different experiment, we choose $\delta_c<0$, $\delta_s\approx+\gamma$, and the spatial phase of the sideband to be $\chi\sim\pi$. Then atoms are always excited from near the tops of the ground-state hills at the carrier's nodes to near the bottom of the excited-state hills (see Fig. 3). This results in still a different form of Sisyphus cooling using this force. A typical single-frame image from Sisyphus cooling is shown in part (a) of Fig. 4 (no averaging). The atomic beam appears as a vertical stripe in the absence of laser light, and its spatial distribution with and without laser cooling is shown in part (b). All atoms within the initial $\sim 5\gamma/k$ wide velocity distribution are cooled by this force, indicating that the velocity capture range of this large force is $\gg\gamma/k$.

We observe transverse cooling of the atomic beam when $\delta_c\approx-40\gamma$ and heating when δ_c has the opposite sign (see Fig. 9). This dependence on the sign of the intense beam's detuning is in direct contrast to Ref. [12] because here the atomic excitation is caused by the weak but nearly resonant sideband near the nodes of the high-intensity carrier standing wave. In Ref. [12], the excitation occurs at the antinodes because there is only one frequency to cause both the light shift and the optical pumping.

Figure 9(a) shows the heating that occurs when $\delta_c>0$. There is also clear evidence of channeling of the low-velocity atoms here that is difficult to distinguish from cooling when $\delta_c<0$. Observation of channeling requires that the sideband is slightly detuned such that the maximum value of γ_p^s is away from the node of the carrier, and therefore atoms with small velocities channeled at the carrier's node will not escape the channel by pumping to the excited state. Atoms with larger velocities are able to climb higher up the light shift potential of the ground state and get pumped to the excited state by the sideband and heated away from $v=0$. In contrast, when the sideband's detuning is very small and the maximum value of γ_p^s is near the node of the carrier, atoms at the node of the carrier will get out of the channel by frequent excitations, where they are at the top of the light shift potential. Figure 9(b) shows heating of the atoms without channeling when $\delta_s=-1\gamma$.

C. Numerical simulations

We performed a numerical simulation of the atomic motion using the energy levels from the doubly dressed atom

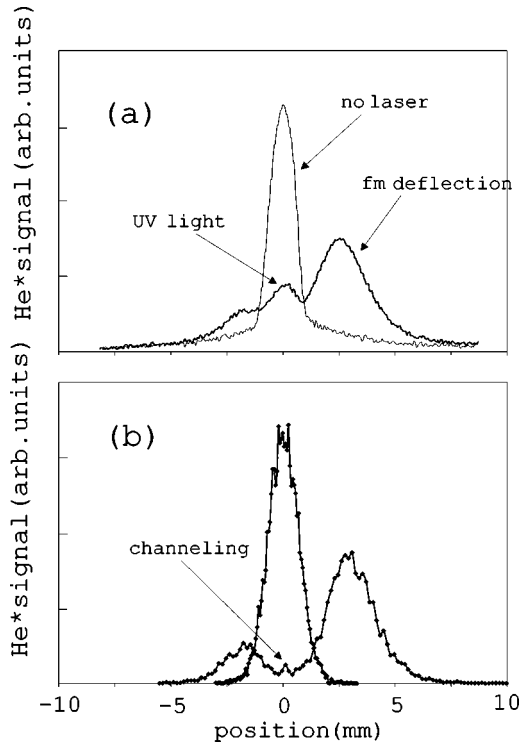

FIG. 10. Part (a) shows the measured spatial distribution (with and without the FM counter-propagating beams) at the detector for the parameters given in Table I. The interaction time is $\approx 35\tau$. The He* source also produces uv light that is detected, and this comprises the dominant part of the peak seen in (a) in the center. The output of the numerical simulation is shown in part (b). The simulation does not include the uv light from the source, but the small, undeflected peak at the center is attributed to very slow atoms in the bottom of the potential that cannot access points (*A*) and (*C*) of Fig. 1 and so are channeled. This part of the signal is obscured by the uv light in the experimental profile.

model of Sec. II C. A classical description of the atomic motion is justified because the width of the velocity distribution is larger than the recoil velocity $v_r \equiv \hbar k/M$. The quantitative agreement between this and our measurements provides corroboration of some of our intuitive ideas. For example, we neglected atomic excitation by the carrier and the simulation shows that this indeed does not affect F_{pop}. It also provides a quantitative demonstration of the asymmetry for $\chi = \pi/4$ that produces the deflection force.

We used a Monte Carlo method to generate the distribution of Landau-Zener transitions for each time an atom encounters an avoided crossing and also to account for spontaneous emission processes. The simulation works with several thousand atoms in a beam that crosses the laser field perpendicular to its $\vec{k}$ vectors. For each atom, the initial position is chosen randomly over an optical wavelength. The initial longitudinal velocity v_l and transverse velocity v follow Gaussian distributions corresponding to our experimental conditions.

The simulation calculates the position and velocity of the atoms. These values are then used to calculate the atoms' final position at the detector which is 70 cm downstream of the interaction region. By plotting the final distribution of atomic positions for different values of Ω_c^0, δ_s, and χ, we obtain qualitative agreement with our measurements, including cooling, heating, and channeling effects. A sample comparison between the experiment and simulation is shown in Fig. 10. We also performed the same Monte Carlo simulation with the energy levels from the effective Hamiltonian of Eq. (9) as discussed above, but this yielded poorer agreement.

IV. CONCLUSION

Use of a second frequency of light to manipulate the strong dipole force can be exploited in several ways. With the bichromatic force of Refs. [2–4], the two optical fields are of comparable intensity and detuning. Rectification of the dipole force by properly chosen laser parameters has been studied in Refs. [5–10]. Here, we choose still different laser parameters and utilize the relative phase of the two standing waves to demonstrate new forms of optical forces. They are shown to be $\gg F_{rad}$ and cover a velocity range $\gg \gamma/k$. We have demonstrated qualitative agreement with an intuitive model of the workings of these forces, including a Sisyphus cooling description. We have also made numerical simulations of the atomic motion in our light fields whose results compare very well with our measurements. We anticipate that further studies of polychromatic forces will continue to expose new and interesting phenomena.

ACKNOWLEDGMENTS

This work was supported by the ONR and ARO.

[1] J. Dalibard and C. Cohen-Tannoudji, J. Opt. Soc. Am. B **6**, 2023 (1989).
[2] M. Williams *et al.*, Phys. Rev. A **60**, R1763 (1999).
[3] M. Williams *et al.*, Phys. Rev. A **61**, 023408 (2000).
[4] M. Cashen and H. Metcalf, Phys. Rev. A **63**, 025406 (2001).
[5] A.P. Kazantsev and I. Krasnov, J. Opt. Soc. Am. B **6**, 2140 (1989); see also Pis'ma Zh. Éksp. Teor. Fiz. **46**, 3333 (1987).
[6] V.S. Voitsekhovich *et al.*, Sov. Phys. Tech. Phys. **33**, 690 (1988).
[7] V.S. Voitsekhovich *et al.*, JETP Lett. **49**, 161 (1989); Sov. Phys. JETP **72**, 219 (1991).
[8] R. Grimm *et al.*, Phys. Rev. Lett. **65**, 1415 (1990).
[9] R. Gupta *et al.*, Phys. Rev. Lett. **71**, 3087 (1993).
[10] T. Grove *et al.*, Phys. Rev. A **51**, R4325 (1995).
[11] S.K. Dutta *et al.*, Phys. Rev. A **62**, 035401 (2000).
[12] A. Aspect *et al.*, Phys. Rev. Lett. **57**, 1688 (1986).
[13] H. Metcalf and P. van der Straten, *Laser Cooling and Trapping* (Springer, New York, 1999).
[14] Neglecting the other sideband has been tested experimentally by combining the carrier beam with a single sideband pro-

duced by an AOM and comparing the results with the EOM measurements. Our results from the two kinds of experiments are indistinguishable.

[15] In the harmonic approximation, the oscillation frequency is $\omega_{osc}=2\sqrt{\omega_{ls}\omega_r}$ ($\sim\gamma$ for our parameters). Here, $\omega_r\equiv\hbar k^2/2M$ is the recoil frequency. Even an atom that arrives in the excited-state potential at rest will move on average $(\omega_{osc}\tau/\pi)(\lambda/2)\sim\lambda/2\pi$ during an excited-state lifetime. Thus, slow atoms are most likely to decay spontaneously to the ground state from a lower position on the potential than point (*D*) of Fig. 1(a), and thereby gain kinetic energy. They will then land on the ground-state potential at a higher energy than the next point equivalent to (*C*) they would encounter, so they are further accelerated to the right.

[16] L. D. Landau and E. M. Lifschitz, *Mechanics*, 3rd. ed. (Pergamon, Oxford, 1976), Sec. 30.

[17] J. Dalibard and C. Cohen-Tannoudji, J. Opt. Soc. Am. B **2**, 1707 (1985).

[18] Z. Ficek and H.S. Freedhoff, Phys. Rev. A **48**, 3092 (1993).

[19] H. Kim *et al*., J. Phys. B **33**, 1703 (2000).

[20] Z. Ficek *et al*., Opt. Spectrosc. **87**, 670 (1999).

[21] C. Cohen-Tannoudji and S. Reynaud, J. Phys. B **10**, 345 (1977).

[22] R. Grimm *et al*., Opt. Lett. **19**, 658 (1994).

[23] Z. Ficek and H.S. Freedhoff, Phys. Rev. A **53**, 4275 (1996).

[24] L. D. Landau and E. M. Lifshitz, *Quantum Mechanics (Non-Relativistic Theory)* (Pergamon, Oxford, 1976); see especially Sec. 90.

[25] Made by Keopsis, Lannion, France.

[26] J. Kawanaka *et al*., Appl. Phys. B: Lasers Opt. **56**, 21 (1993).

[27] H. Mastwijk *et al*., Eur. Phys. J. D **4**, 131 (1998); H. Mastwijk, Ph. D. thesis, University at Utrecht, 1997.